NBSIR 75-661

Strength Degradation of Brittle Surfaces: Sharp Indenters

B. R. Lawn, E. R. Fuller, and S. M. Wiederhorn

Inorga
Institu
Nation
Washi

May 1

Interi

Prepared for
Department of the Navy
Office of Naval Research
Arlington, Virginia 22217

NBSIR 75–661

STRENGTH DEGRADATION OF BRITTLE SURFACES: SHARP INDENTERS

B. R. Lawn, E. R. Fuller, and S. M. Wiederhorn

Inorganic Materials Division
Institute for Materials Research
National Bureau of Standards
Washington, D.C. 20234

May 1975

Interim Report for Period July 1, 1974 through June 30, 1975

Prepared for

Department of the Navy
Office of Naval Research
Arlington, Virginia 22217

U.S. DEPARTMENT OF COMMERCE, Rogers C.B. Morton, Secretary

NATIONAL BUREAU OF STANDARDS, Richard W. Roberts, Director

STRENGTH DEGRADATION OF BRITTLE SURFACES:

SHARP INDENTERS

B. R. Lawn*, E. R. Fuller, and S. M. Wiederhorn

Institute for Materials Research
National Bureau of Standards
Washington, D. C. 20234, U.S.A.

*On study leave, from School of Physics, University of New South Wales, Kensington, N.S.W. 2033, Australia

Abstract

A theory of strength loss for brittle surfaces in contact situations, developed in a previous paper for "blunt" indenters, is here extended to the case of "sharp" indenters. A prior fracture mechanics analysis of crack growth beneath ideal cone indenters serves as the basis for predetermining the prospective surface degradation of ceramic components in service. Compared to blunt indenters, severe degradation can occur at lower contact loads. However, at high loads the extent of degradation becomes remarkably insensitive to details in the indenter geometry. Essential theoretical predictions are verified by bend tests on glass slabs. The effect of indenter "sharpness" and initial specimen surface flaw state are investigated systematically, along with some secondary rate effects in the contact process. The possibility of minimizing degradation via adjustment of material parameters (including hardness) or surface condition (e.g., residual stresses, frictional properties) is briefly discussed.

I. Introduction

In a previous paper[1] an analysis was presented of the degradation incurred by brittle surfaces under circumstances in which indenting particles could be considered "blunt". The classical Hertzian cone crack produced beneath a hard sphere was adopted as a model representation of this situation. "Real contact" situations involving irregular particles fall somewhere between this and a second limiting type of indentation configuration, namely configurations in which the particles may be viewed as "sharp" (i.e., possessing an ideally sharp point). The contact conditions, and hence the ensuing indentation fracture patterns, are somewhat different in this second case, and are not as well understood as in the cone crack configuration. Nevertheless, recent fracture mechanics studies of sharp-indenter systems[2-4] provide us with an adequate basis for predicting degradation behavior. The present study is directed toward this end, and accordingly serves to complement the earlier study.[1]

Because the deformation beneath a perfectly sharp indenter cannot be completely elastic (as it can beneath a blunt indenter), we must expect some new features in the degradation properties of a given brittle material. We shall indeed show this to be the case, particularly in the initiation stages of indentation fracture at low loads. At the same time, once the crack system develops well beyond the contact zone it might be anticipated that the influence of indenter geometry will become less marked. Again, we shall demonstrate this to be so. Considerations along these lines are useful in any discussion of damage in real contact processes.

As before, it will be assumed that quasistatic conditions prevail throughout the indentation process. Ideally rigid cones will be taken as typifying the sharp-indenter configuration.

II. Point Indenters and Median Penny Cracks

Let us examine the essential features of the crack pattern produced in a brittle surface loaded with a hard, sharp point indenter. The solution for the linear elastic stress field in the indented specimen prior to cracking contains a singularity about the contact point, and has an inverse-square fall-off with the radial distance.[2, 3] Removal of this singularity is accounted for physically by the formation of an irreversible, stress-relieving zone of deformation (plastic or viscous flow, structural densification, etc.) around the contact; the intensity of the local stresses (characterized by the mean contact pressure) at which this deformation occurs determines the hardness of the material. The stress concentration immediately below the indenter point nevertheless remains high, and downward-extending cracks can be nucleated at very low loads, depending on the degree of brittleness. This represents a major departure from the blunt-indenter case, where pre-present surface flaws control the crack initiation process. Indeed, if the tip region of the indenter is somehow bluntened, or if the pre-present flaws are sufficiently large, the formation of a small cone crack may precede the development of the deformation-induced cracks: this is a complication which we take up again later (Section IV), but which for the present may be ignored.

Once the cracks have been nucleated, they extend downward on median planes in accordance with the scheme of Fig. 1. Several mutually intersecting median cracks (depending, for example, on the symmetry

of the indenter or the anisotropy of the specimen) may propagate simultaneously. However, we shall focus attention on a single crack system, noting from empirical observation that the depth of cracking is not too sensitive to the number of cracks formed.[4] We describe the variation of median-crack depth with load for the following stages in the growth:[4]

(1) Formation of "contained" median penny crack

Whereas in reality the nucleation of median cracks involves a threshold in the loading, for the most brittle ceramic materials this threshold is insignificantly small (typically less than one newtron, as is readily evident from hardness test observations). The cracks assume the form of well-defined pennies, wholly contained below the contact zone, and grow downward stably as the load is applied. This configuration constitutes a complex elastic-plastic problem, for which an exact solution is out of the question. A simplified fracture mechanics analysis[2] indicates that in addition to the usual fracture parameters, namely the fracture surface energy Γ and the Young's modulus E, the hardness H should enter into the relationship between indenter load and crack size; the scale of the deformation zone determines the degree of stress relief that occurs about the singular point in the ideally elastic field. A second analysis, based on a more or less dimensional argument for general penny-shaped cracks, predicts a slightly different relationship between the parameters.[4] Although less explicit in the dependence on hardness, the second treatment provides a better empirical fit to crack growth data, and will thus be cited here.

Accordingly, we find, for smooth indenters,

$$P^2/D^3 = 2\Gamma E/\kappa_D^f(\nu, H/E, \psi) \qquad (1)$$

where P is the load on the indenter, D is the depth of the crack (the penny daimeter for the contained median penny crack), ν is Poisson's ratio, ψ is the cone half-angle and κ_D^f is a dimensionless factor (f signifying formation stage of crack growth) whose value needs to be determined by experimental calibration. It may be noted that this equation does not involve the state of the specimen surface (flaw population, etc.). However, the angle of the cone, through its influence on the indentation field, does enter as a variable.

Up to this point the cracks cannot be considered to be "well-developed," for they still remain within the sphere of influence of the nucleation zone immediately below the contact. However, there is a critical configuration, albeit ill-defined, above which the contact zone can no longer contain the expanding penny ($D>>a$, Fig. 1)*. At this point the crack "breaks through" to the specimen surface, and thereby becomes fully propagating.

(2) Propagation of "center-loaded" median half-penny crack

Beyond the breakthrough load the median crack assumes the form of a center-loaded half-penny crack (radius D, Fig. 1). Details of events at the contact zone no longer exert a strong influence on the fracture mechanics: the crack has escaped the nucleation forces, and

*This in turn implies a critical load, since, taken together with the definition of hardness, $H = P/\alpha\pi^2$ (α a geometrical factor, which is unity for cone indenters), Eqn. (1) predicts, for a fixed value of H, $D/a \propto P^{1/6}$.

is now controlled by the component of the applied load which acts to wedge open the mouth region. Nevertheless, the crack geometry retains the essential features of a (somewhat modified) penny configuration, in which case we may predict for smooth indenters, in analogy with Eqn. (1), the relation

$$P^2/D^3 = 2\Gamma E/\kappa_D^p(\nu,\psi) \tag{2}$$

with κ_D^p another dimensionless factor (p signifying propagation stage of crack growth); we note that the hardness now disappears from the fracture mechanics calculation. A straightforward analysis, based on a center-loaded, full penny in an infinite solid, gives[4]

$$\kappa_D^p(\nu,\psi) = (1-\nu^2)/\pi^3 \tan^2\psi. \tag{3}$$

Generally, the contact will not be smooth. It can be shown that the effect of including frictional tractions at the indenter-specimen interface is simply to replace ψ by $\psi' = \psi + \arctan \mu$ (μ = coefficient of friction), i.e., effectively to "blunt" the indenter tip.[4] The effect of ignoring friction is therefore to overestimate κ_D^p in Eqn. (3), and hence D in Eqn. (2). In other words, we deal with a "worst case" situation.

In practice, the transition from stage (1) to stage (2) in the growth of a given median crack can be detected, either by direct observation of the indentation process (in transparent solids), by monitoring the acoustic emissions as the contained penny pops through to the specimen surface, or by recording load drops in a fixed-grips loading arrangement.[4] While such discontinuities in growth occur at generally lower critical loads as the cone half-angle diminishes, the critical loads themselves vary considerably

under apparently constant indentation conditions. Moreover, mutually intersecting median cracks may "pop-in" at different stages in the loading, and accordingly be retarded in further growth by their less-developed neighbors. Multiple-cracking complications are particularly noticeable at the lower cone angles. This aspect of the indentation cracking remains poorly understood.

(3) The residual median crack

Unlike the elastic-brittle contact of the ideally blunt indenter situation,[1] the present case is complicated by further developments in the crack pattern upon unloading. Incompatibility between the stress-strain responses of nonlinear material within the irreversible deformation zone and linear material without gives rise to mismatch tractions at the contracting zone boundary. The net result is a residual stress field which begins to dominate the field of the applied loading just prior to complete removal of the indenter. This residual field contains a component of tension sufficiently intense to generate an entirely new, laterally-extending system of cracks.[2, 5] However, such lateral cracks are relatively shallow, and thus do not contribute significantly to degradation. A more important influence of the residual stresses here is evident in the behavior of contained penny cracks already formed during the preceding, loading half-cycle. These cracks progressively grow toward the specimen surface as the indenter is withdrawn; an alternative route to the fully-developed form thereby exists, without the need for the critical pop-in load ever to be exceeded.[4]

Thus the final state of the strength-controlling median crack system inevitably approaches the half-penny configuration, regardless of the loading history. This is most commonly evidenced by the appearance of characteristic radial traces of the median cracks on the indented surfaces. The dimensions of these traces tend to reflect the depth of cracking one would anticipate if the half-penny configuration were to be realized prior to maximum loading.[4] With this information we may sensibly make use of Eqn. (3) for fully-developed median cracks to determine the effect of indenter "sharpness" (all else being constant) on the resultant crack size. Fig. 2 is an appropriate plot of $[\underline{\kappa}_D^p(\underline{\psi})]_\nu$ for cone indenters on glass, with $\underline{\nu} = 0.25$. Experimental data from indentation observations, for tungsten carbide indenters on glass surfaces in air environments, fall somewhat below the calculated curve, suggesting that the effects of friction are not insignificant here. Nevertheless, we shall proceed for the present on the basis of a smooth contact, mindful that the resulting upper limit $\underline{\kappa}_D^p(\underline{\psi})$ to be used in Eqn. (2) will lead to an overestimate in $\underline{D}$, thus providing a conservative value for the strength of the indented surface.

III. Strength Degradation Tests

(1) Test procedure

The standard Griffith formula for the rupture stress $\underline{\sigma}$ in a homogeneous tensile field once again provides the basis for the strength tests:

$$\sigma = [2\Gamma E/\pi(1-\nu^2)c_f]^{1/2} \qquad (4)$$

where c_f is the effective flaw size of an equivalent through crack. Of the variables in Eqn. (4), it is the flaw size which is most widely susceptible to extraneous influences (mechanical, thermal, chemical, etc.).

Soda-lime silicate glass laths for four-point bend testing were prepared in much the same manner as in the previous study,[1] with one or two minor differences. In the present case, the 10 μm level of pre-present flaws typical of carefully handled ceramic surfaces is eclipsed by the extent of median cracking produced at indentation loads as low as 1N. As-received laths hence provided perfectly adequate test surfaces for the bulk of the testing, although the test areas of one set of specimens were pre-abraded by a grit-blast treatment[1] to determine whether severe pre-present surface damage produces any side-effects in the indentation process.

For each specimen the prospective indentation site was covered with a drop of paraffin oil to prevent moisture-assisted slow crack growth during subsequent testing. (In the case of grit-blasted specimens, the abraded area was covered immediately after the treatment.) Each specimen surface was then indented with a tungsten carbide conical indenter of given half-angle ψ, at a prescribed load P. (The tip radius of the cones used never exceeded 5 μm throughout the experiments.) The specimens were then loaded to rupture with the indented surface in tension. Unless specified otherwise, the bend test was effected within four hours of indenting in the experiments to be reported here.

Examination of the laths after breaking indicated the indentation site to be the origin of fracture in the vast majority of tests. Isolated edge failures did occur, and these were rejected from the data accumulation. Reproducibility in strength values was limited mainly by variations in the indentation crack pattern under any specified set of test conditions; the scatter in data points in the figures to follow therefore serve to indicate the experimental accuracy.

(2) Strength of indented test pieces

Strength degradation was investigated as a function of indentation load, for different cone half-angles. Up to a (very low) limiting load, $\underline{P}'$ say, the rupture stress maintained the level characteristic of the unindented surface (depending on the prior history of the glass specimens). In this region of behavior the effective length of the dominant flaw is presumably determined by the size of pre-present microcracks, i.e., $\underline{c}_f = \underline{c}_f^o$ say, $(\underline{P} \leqslant \underline{P}')$. Above the limiting load the rupture stress declined steadily. The effective flaw length here becomes a function of the size of median cracks, i.e., $\underline{c}_f = \underline{c}_f(\underline{D})$, $(\underline{P} > \underline{P}')$: an analysis of penny cracks in a tensile field gives the explicit relation $\underline{c}_f \approx (4/\pi^2)\underline{D}$ (Appendix). With Equation (2), this result allows us to rewrite the strength equation (4) in terms of indentation load, for a given cone, under fixed test conditions,

$$\sigma = [2\Gamma E/\pi(1-\nu^2)c_f^o]^{1/2} \qquad (P \leqslant P') \qquad (5a)$$

$$\sigma = \{(2\Gamma E)^{2/3}\, \pi^{1/2}/2(1-\nu^2)^{1/2}[\kappa_D^p(\nu,\psi)]^{1/6}\}P^{-1/3} \qquad (P > P'). \qquad (5b)$$

An evaluation of these equations may be carried out in terms of readily measurable fracture mechanics parameters. For tungsten

cone indenters on soda-lime glass we take the following values:
$\underline{E} = 7.0 \times 10^{10}$ Nm^{-2}, $\underline{\nu} = 0.25$ and $\underline{\Gamma} = 3.9$ Jm^{-2} (glass data[6]);
$\underline{K}_D^P$ (30°) $= 9.0 \times 10^{-2}$, $\underline{K}_D^P$ (40°) $= 4.3 \times 10^{-2}$, $\underline{K}_D^P$ (50°) $= 2.0 \times 10^{-2}$,
$\underline{K}_D^P$ (60°) $= 1.1 \times 10^{-2}$, $\underline{K}_D^P$ (70°) $= 5.0 \times 10^{-3}$, $\underline{K}_D^P$ (80°) $= 1.5 \times 10^{-3}$
(as per the curve in Fig. 2). This then leaves $\underline{c}_f^o$ and $\underline{\psi}$ as test variables, of which the second has the more interesting implications.

(a) Effect of flaw size. A preliminary indentation/strength test run was conducted to check the effect of initial surface state on degradation. Fig. 3 compares results for surfaces as-received and grit-blasted (No. 100 SiC grit, corresponding to $\underline{c}_f^o = (23 \pm 5)\mu m$)[1], for a cone of half-angle 70°. Also included in the figure are the theoretical predictions (full lines) of Eqn. 5a and 5b. Other than at low loads, where the abrasion flaws dominate the indentation damage in the case of grit-blased surfaces, the results are indistinguishable. Consequently, for the remainder of the tests it suffices to work simply with as-received surfaces.

(b) Effect of cone angle. The most extensive runs were directed to an investigation of the role of indenter sharpness in surface degradation. Fig. 4 illustrates the experimental data (points), along with the theoretical curves (full lines) from Eqn. (5). Agreement here is reasonable, taking into account the spread in the data, although some discrepancy is apparent at the largest cone angle, $\underline{\psi} = 80^o$. We should note that the strength behavior is not highly sensitive to indenter sharpness, except perhaps again at the larger angles, notably at $\underline{\psi} = 80^o$. We may note further that the strength fall-off is remarkably slight with increasing indenter load. That the loads attained in

these experiments are substantial is borne out by the fact that the sharper cones quickly became rounded (in which case their tips were reground), and the glass beneath the contact began to crush, at levels not much higher than those represented in Fig. 4.

(c) Some secondary, rate effects. Finally, two interesting time-dependent effects observed by Holland and Turner[7] in analogous strength-loss tests on scratched glass surfaces, were briefly examined. In the first, Holland and Turner noted a tendency for specimens to slowly recover their strength as the delay between indentation and rupture in bending was prolonged. Fig. 5 confirms this effect, for the specific case of normal indentation at $\psi = 70°$, $P = 100$ N. However, the recovery is significant only for aging times of a day or more, and therefore does not enter as a factor in the results reported earlier in this study.

In the second effect, which relates to load rate effects, Holland and Turner reported a drop of about twenty per cent in strength values as the scratch velocity was increased over a range 0-5 ms^{-1}, at normal load $P = 5$ N. Results of a parallel experiment, in which the crosshead speed to a peak (quasistatic) normal indentation load $P = 100$ N was varied over four orders of magnitude, are shown in Fig. 6. This time there is no evidence of a rate effect.

IV. Discussion

The present model establishes a basis for predicting a priori the prospective strength degradation in contact situations where the indenting particles can be considered "sharp". Comparing the

strength equation (5) with its counterpart for blunt indenters in the earlier study,[1] we find again that degradation is minimized for surfaces of large characteristic $\underline{\Gamma}$ (tough), $\underline{E}$ (stiff) and $\underline{\nu}$ (tension-inhibiting, in basically compressive loading). Further, we might anticipate, following the description of Section II (1), low values of $\underline{H}$ to be of advantage in suppressing the formation of indentation-induced cracks at low loads; we shall say a little more about the role of hardness again later.

A major distinction between the cases of sharp and blunt indenters arises in connection with the state of the brittle surface prior to indentation. Whereas with blunt indenters pre-existing surface flaws exert an important influence through control of fracture initiation processes, the same is not true with sharp indenters, which induce their own flaws. On the other hand, there are other aspects of the surface condition which may have significant effects in crack initiation independently of indenter geometry. An example is the fracture-inhibiting effect of residual compressive stresses in a toughened surface. All such effects will be manifest at lower indentation loads, where the indentation cracks remain within the sphere of influence of the near-contact region. Generally, however, it is found that the more pointed indenters, by virtue of their greater capacity to concentrate stresses, always produce the most severe damage in this domain.

At higher loads the differences due to details in the near-contact conditions tend to "wash out." In their well-developed form, all indentation cracks inevitably assume some modified penny configuration,[4]

the growth of which becomes determined by the stresses of "point loading". The field in this limit is radial (inverse-square fall-off) about the contact point, which explains the parallel behavior, toward the upper end of the indentation load scale, between the strength-loss curves in Fig. 4 of the present paper and Figs. 3 and 4 of Ref. 1. There is accordingly less need to take into account specifics of indenter geometry when the contact damage is severe. Moreover, while sharper indenters do tend to produce deeper cracks at a given load,[4] these same indenters tend also to become flattened at the tip, or to crush severely the supporting surface. Further, to produce these deeper cracks the sharper indenter must penetrate further between the crack walls, i.e., it must do more work. The implication here is that in situations in which the indentation event is governed by a fixed energy input (e.g., in a fixed-velocity impact situation) the effects of indenter sharpness may well disappear altogether.[8]

Nevertheless, taking a broad view of the strength degradation curves obtained in this and the earlier study, the degree of indenter sharpness, as signified by the cone half-angle (or sphere radius), remains an important factor to be considered. This is particularly so in relation to the interpretation of degradation processes in "real contact situations"; here it may be feasible to characterize a sharp indenting particle by some "effective half-angle" (we may note, for instance, that a Vickers pyramid, whose opposing diagonals subtend an angle of 136°, produces cracks in glass of very much the same depth as does a cone of $\underline{\psi} = 70°$[4]). However, in most cases the

assignment of a simple index of sharpness will not be so straightforward. Even the sharpest particles must in reality have a finite non-zero tip radius, so the possibility exists of a gradual "blunt-sharp transition" in the strength response with increasing severity of indentation.* An opposite, "sharp-blunt transition", corresponding to an increasing argument in the tangent term of Eqn. (3), may be realized in cases where frictional effects become pronounced.** The most general real contact situation is clearly very complex indeed.

Friction is a further factor which warrants a good deal more attention than we have been able to give here. It should be re-emphasized that the present tests were conducted under oil. In a different environment the frictional properties of the indenter/specimen contact interface could be quite different. In most instances it would be wise to base any strength design criterion on the conservative assumption that frictional tractions are entirely absent (thereby overestimating the depth of indentation cracking). On the

---

*The corresponding change in fracture pattern in such a case has been well demonstrated by K. Phillips, whose results are illustrated in Fig. 21 of Ref. 3.

**As mentioned in Section II (2), the effective cone angle $\underline{\psi}'$ when friction is present is $\underline{\psi}$ + arctan $\underline{\mu}$. Thus for the indentations corresponding to $\underline{\psi}$ = 80° in the present experiments, a friction coefficient $\underline{\mu} \approx 0.2$ gives $\underline{\psi}' \approx 90°$, a "perfectly blunt" indenter. In this one case examination of the cone-indented specimens revealed Hertzian cone fracture, typical of ideally blunt indenters, to form at the expense of the median fracture system.[4] The data points in the plot for $\underline{\psi}$ = 80° in Fig. 4 do in fact fit reasonably well to the degradation curve predicted for well-developed cone cracks.[1] In this description the cone-crack curve provides an upper limit to the strength resulting from any sharp-point contact situation.

other hand, the possibility is raised of fabricating surfaces in such a way that the operative frictional forces are deliberately made large, in order to suppress the relatively dangerous median fracture system.

Finally, there are a number of secondary effects associated with non-equilibrium, and history-dependent, crack configurations. Several of these effects have been discussed in the earlier work,[1] and we need only briefly consider one new aspect here. We have already indicated the possible role of the irreversible deformation properties of the indented solid, as characterized by the hardness, in controlling the initial stages of crack growth. The hardness of glasses[9] and many other brittle materials[10] is strongly rate-dependent, so we might expect to observe additional kinetic effects in the strength degradation curves, particularly at lower loads where the inelastic processes appear to have some influence on the crack formation (Sections II (1), II (3)). The null effect observed in Fig. 6 may arise from the fact that our tests were conducted under oil, an environment which tends to minimize the time dependence of the hardness of glass.[9] The analogous experiments by Holland and Turner (Section III), on the other hand, were conducted in an ordinary laboratory atmosphere: their positive effect, in which the strength was observed to diminish with velocity of the scratch indenter, correlates with a corresponding increase in hardness of glass with decreasing contact duration in air.[9] This is one interesting aspect which invites further, special attention, particularly in connection with less brittle ceramic materials.

Acknowledgements

The authors are grateful to A. G. Evans for stimulating discussions relating to this work. Sponsorship through the Office of Naval Research under Contract No. NR-032-535 is acknowledged.

Appendix

Let us examine the mode of failure of a well-developed median half-penny crack in a uniform tensile stress field. In the most general case, the median plane of the crack will be inclined at some angle, β say, to the tensile axis, as in Fig. A1. We anticipate that full-scale fracture will initiate at points on the crack perimeter coincident with the specimen surface (point A). For completeness, however, a general point P will be considered.

The procedure follows that outlined in the Appendix of the earlier paper for cone cracks.[1] For inclined penny cracks in uniaxial tensile fields the standard stress-intensity factors at a prospective extension point, P, are[11]

$$K_I = 2\sigma\,(D/\pi)^{1/2}\sin^2(\beta)$$

$$K_{II} = 2\sigma\,(D/\pi)^{1/2}\sin(2\beta)\cos(\zeta)/(2-\nu) \qquad \text{(A1)}$$

$$K_{III} = 2\sigma\,(D/\pi)^{1/2}(1-\nu)\sin(2\beta)\sin(\zeta)/(2-\nu)$$

where the subscripts denote I, "opening", II, "sliding", and III, "tearing", modes of fracture. (These solutions omit a small correction factor due to the presence of the free specimen surface in the half-penny configuration.) The action of the shearing stresses in the general crack orientation is to direct the crack-plane extension through some energetically favorable tilt angle θ and twist angle ϕ. At point A, this extension will only consist of a tilt; whereas at point B, it will only consist of a twist (Fig. A1). Considering just an incremental extension, we identify opening, sliding, and tearing types of local stresses in the prospective crack plane:

$$
\begin{aligned}
\sigma_{y'y'} &= g_I^{\ I}\,[K_I/(2\pi r)^{1/2}] + g_I^{\ II}\,[K_{II}/(2\pi r)^{1/2}] + g_I^{\ III}\,[K_{III}/(2\pi r)^{1/2}] \\
&= K'_I/(2\pi r)^{1/2}, \\
\sigma_{x'y'} &= g_{II}^{\ I}\,[K_I/2\pi r)^{1/2}] + g_{II}^{\ II}\,[K_{II}/(2\pi r)^{1/2}] + g_{II}^{\ III}\,[K_{III}/2\pi r)^{1/2}] \\
&= K'_{II}/(2\pi r)^{1/2}, \qquad \text{(A2)} \\
\sigma_{y'z'} &= g_{III}^{\ I}\,[K_I/(2\pi r)^{1/2}] + g_{III}^{\ II}\,[K_{II}/(2\pi r)^{1/2}] \\
&\quad + g_{III}^{\ III}\,[K_{III}/(2\pi r)^{1/2}] \\
&= K'_{III}/(2\pi r)^{1/2},
\end{aligned}
$$

where x', y', z' are the coordinates in a system of the prospective crack plane and the "transformed stress-intensity factors" $\underline{K}'_I$, $\underline{K}'_{II}$, and $\underline{K}'_{III}$ define the field for the modified crack. The $\underline{g}$ terms are calculable by transforming the angular-dependent components of the standard crack-tip stress expressions.[12] For plane strain we obtain

$$
\left.
\begin{aligned}
g_I^{\ I} &= \cos\left(\tfrac{\Theta}{2}\right)\left[\cos^2\left(\tfrac{\Theta}{2}\right)\cos^2(\phi) + 2\nu\sin^2(\phi)\right] \\
g_{II}^{\ I} &= \sin\left(\tfrac{\Theta}{2}\right)\cos^2\left(\tfrac{\Theta}{2}\right)\cos(\phi) \\
g_{III}^{\ I} &= -\cos\left(\tfrac{\Theta}{2}\right)\left[\cos^2\left(\tfrac{\Theta}{2}\right) - 2\nu\right]\sin(\phi)\cos(\phi)
\end{aligned}
\right\} \quad \text{(mode I)} \qquad \text{(A3)}
$$

$$
\left.
\begin{aligned}
g_I^{\ II} &= -\sin\left(\tfrac{\Theta}{2}\right)\left[3\cos^2\left(\tfrac{\Theta}{2}\right)\cos^2(\phi) + 2\nu\sin^2(\phi)\right] \\
g_{II}^{\ II} &= \cos\left(\tfrac{\Theta}{2}\right)\left[3\cos^2\left(\tfrac{\Theta}{2}\right) - 2\right]\cos(\phi) \\
g_{III}^{\ II} &= \sin\left(\tfrac{\Theta}{2}\right)\left[3\cos^2\left(\tfrac{\Theta}{2}\right) - 2\nu\right]\sin(\phi)\cos(\phi)
\end{aligned}
\right\} \quad \text{(mode II)} \qquad \text{(A4)}
$$

$$
\left.
\begin{aligned}
g_I^{\ III} &= \cos\left(\tfrac{\Theta}{2}\right)\sin(2\phi) \\
g_{II}^{\ III} &= \sin\left(\tfrac{\Theta}{2}\right)\sin(\phi) \\
g_{III}^{\ III} &= \cos\left(\tfrac{\Theta}{2}\right)\cos(2\phi)\,.
\end{aligned}
\right\} \quad \text{(mode III)} \qquad \text{(A5)}
$$

Combining (A2) and (A1) gives

$$K'_\alpha(\beta,\zeta,\Theta,\phi) = 2\sigma(D/\pi)^{1/2}[g_\alpha^{I}\sin^2(\beta) + g_\alpha^{II}(\frac{1}{2-\nu})\sin(2\beta)\cos(\zeta)$$

$$+ g_\alpha^{III}(\frac{1-\nu}{2-\nu})\sin(2\beta)\sin(\zeta)], \tag{A6}$$

where α represents I, II, or III.

From the stress-intensity factors the mechanical-energy-release rate G, per unit width of crack front, follows:

$$G(\beta,\zeta,\Theta,\phi) = [(1-\nu^2)/E][K_I'^2 + K_{II}'^2 + \frac{1}{(1-\nu)}K_{III}'^2]. \tag{A7}$$

For a specific crack angle $\underline{\beta}$, we postulate that the crack at point $\underline{P}$ on the crack perimeter will extend at the tilt angle Θ^* and twist angle $\underline{\phi}^*$ for which the energy release $\underline{G}^*(\underline{\beta},\underline{\zeta})$ is greatest[12], i.e.,

$$\partial G/\partial\Theta = 0 \quad \text{and} \quad \partial G/\partial\phi = 0. \tag{A8}$$

From Eqns. (A3) - (A8) we may compute the required energy term in the form

$$G^*(\beta,\zeta) = [4(1-\nu^2)\sigma^2 D/\pi E]\omega(\beta,\zeta) \tag{A9}$$

where $\underline{\omega}(\underline{\beta},\underline{\zeta})$ is a dimensionless constant that attains a limiting value of unity for $\underline{\beta} = \pi/2$ (independent of $\underline{\zeta}$). It remains to determine the point $\underline{P}$ on the crack perimeter from which the crack will first extend. As before, this is determined by the angle $\underline{\zeta}^*$ which maximizes the energy release rate $\underline{G}^*(\underline{\beta},\underline{\zeta}^*)$.

By introducing the Griffith energy-balance condition for equilibrium cracks,

$$G^* = 2\Gamma, \tag{A10}$$

and writing

$$c_f' = (4/\pi^2)D\,\omega(\beta,\zeta^*), \tag{A11}$$

we can combine with Eqn. (A9) to reproduce the strength equation (4) of the text. The quantity

$$c_f/D = (4/\pi^2)\ \omega(\beta,\zeta^*) \equiv \Omega(\beta,\zeta^*) \qquad \text{(A12)}$$

accordingly determines the effectiveness of the inclined half-penny crack as a critical flaw in the strength test. The quantity $\underline{\Omega}(\underline{\beta},\underline{\zeta})$, is plotted for several values of $\underline{\zeta}$ in Fig. A2 for $\underline{\nu} = 0.25$ (glass value). The corresponding tilt angle $\underline{\Theta}^*$ and twist angle $\underline{\phi}^*$ are plotted in Figs. A3 and A4, respectively. [At point A on the crack perimeter ($\underline{\zeta} = 0°$) there is no twist (i.e., $\underline{\phi}^* = 0°$) and at point B ($\underline{\zeta}=90°$) there is no tilt (i.e., $\underline{\Theta}^*=0°$).] It is seen from Fig. A2 that $\zeta^*= 0$, and as speculated, full-scale fracture commences at point A on the crack perimeter (assuming the correction for the free specimen surface is approximately constant along the perimeter). However, the variation of $\underline{\Omega}(\underline{\beta},\underline{\zeta})$ with $\underline{\zeta}$ is small, when the median crack plane is close to normal coincidence with the uniform tensile stress field.

In practice, it is generally found that the sharp indenter crack pattern contains several intersecting median vents. This is certainly true of the cone indentation of glass, where a minimum of six "arms" in the surface trace pattern is usual.[3] (In certain circumstances, where anisotropic effects in the indentation process are very strong, a single median crack may be produced, but this is very much the exception.) Typically, then, the probability of finding a median crack lying within 30° or so of the most favorable, normal orientation is sufficiently high that the value $\underline{\Omega}(\beta = 90°) = 4/\pi^2$ provides a reasonably accurate assessment of the effective flaw size.

References

1. B. R. Lawn, S. M. Wiederhorn and H. H. Johnson, "Strength Degradation of Brittle Surfaces: Blunt Indenters," J. Am. Ceram. Soc., submitted for publication.
2. B. R. Lawn and M. V. Swain, "Microfracture Beneath Point Indentations in Brittle Solids," J. Mater. Sci., in press.
3. B. R. Lawn and T. R. Wilshaw, "Indentation Fracture: Principles and Applications," J. Mater. Sci., in press.
4. E. R. Fuller and B. R. Lawn, "Fracture Mechanics of Penny-like Cracks in Indentation Cracking," in preparation.
5. B. R. Lawn, M. V. Swain and K. Phillips, "On the Mode of Chipping Fracture in Brittle Solids," J. Mater. Sci., in press.
6. S. M. Wiederhorn, "Fracture Surface Energy of Glass," J. Am. Ceram. Soc., 52 [2] 99-105 (1969).
7. A. J. Holland and W. E. S. Turner, "The Effect of Transverse Scratches on the Strength of Sheet Glass," J. Soc. Glass Tech., 21 383-394 (1937).
8. S. M. Wiederhorn and Brian Lawn, unpublished work.
9. S. P. Gunasekera and D. G. Holloway, "Effect of Loading Time and Environment on the Indentation Hardness of Glass," Phys. and Chem. Glasses, 14 [2] 45-52 (1973).
10. R. E. Hanneman and J. H. Westbrook, "Effects of Adsorption on the Indentation Deformation of Non-metallic Solids," Phil. Mag., 18 [151] 73-88 (1968).

11. M. K. Kassir and G. C. Sih, "Three-dimensional Stress Distribution Around an Elliptical Crack Under Arbitrary Loadings," Trans. A.S.M.E.: J. Appl. Mech., 33 1-11 (1966).

12. B. R. Lawn and T. R. Wilshaw, Fracture of Brittle Solids, Cambridge University Press, Cambridge, 1975, Ch. 3.

Figure Captions

1. Median crack parameters. Crack nucleates at extremity of deformation zone below indenter point, and forms into a penny wholly contained beneath contact surface (broken circle). At some critical load the crack breaks through spontaneously to the free surface ("pop-in"), usually with an attendant increase in crack depth $\underline{D}$, and transforms into a well-developed half-penny configuration (full semicircle). This transformation may also be effected in an alternative, stable manner, via the action of residual stresses about the deformation zone, upon unloading the indenter prior to pop-in.

2. Plot of $\underline{\kappa}_D^p(\underline{\psi})$ from Eqn. (3) (full line) for glass. Data points (circles) represent measurements, using tungsten carbide indenters, made in air.[4]

3. Strength of soda-lime glass surfaces as function of indentation load, for given WC cone, $\underline{\psi} = 70°$. Surfaces both as-received and abraded with No. 100 SiC grit. Oil environment. Crosshead speed of 0.5 mm min^{-1} for indentation tests and 50 mm min^{-1} for bend tests.

4. Strength of as-received soda-lime glass surfaces as function of indentation load, for WC cones of different half-angles (indicated). Oil environment. Crosshead speed: 0.5 mm min^{-1} for indentation tests; 50 mm min^{-1} for bend tests.

5. Strength of as-received soda-lime glass surfaces as function of aging time between indentation and bend testing. Data for WC cone $\underline{\psi} = 70°$, $\underline{P} = 100$ N, oil environment. Crosshead speed: 0.5 mm min^{-1}

6. Strength of as-received soda-lime glass surfaces, as function of crosshead speed in indentation test. Data for WC cone $\underline{\psi}$ = 70°, P = 100 N, oil environment. Crosshead speed for bend tests 50 mm min^{-1}.

A1. Half-penny configuration of median crack, (a) plane view, (b) side view. One seeks the crack increment orientation $\underline{\theta}$ and $\underline{\phi}$ which optimizes the energy release.

A2. Angular terms for median-crack extension in tensile field at several points ($\underline{\zeta}$ = 0°, 45°, and 90°) on the crack perimeter.

A3. Tilt angle, $\underline{\theta}^*$, of median-crack extension in tensile field.

A4. Twist angle, $\underline{\phi}^*$, of median-crack extension in tensile field.

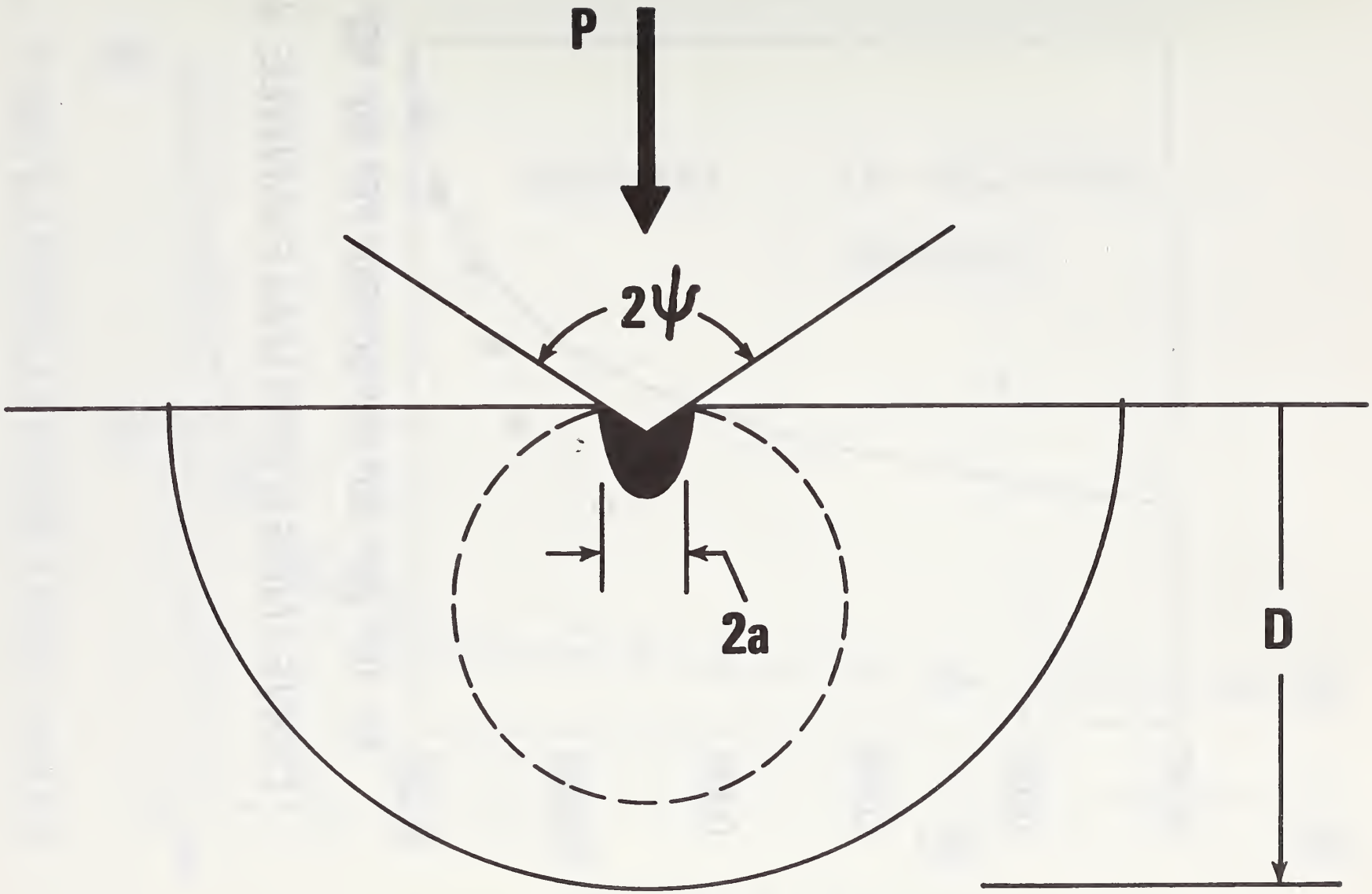
P
2ψ
2a
D

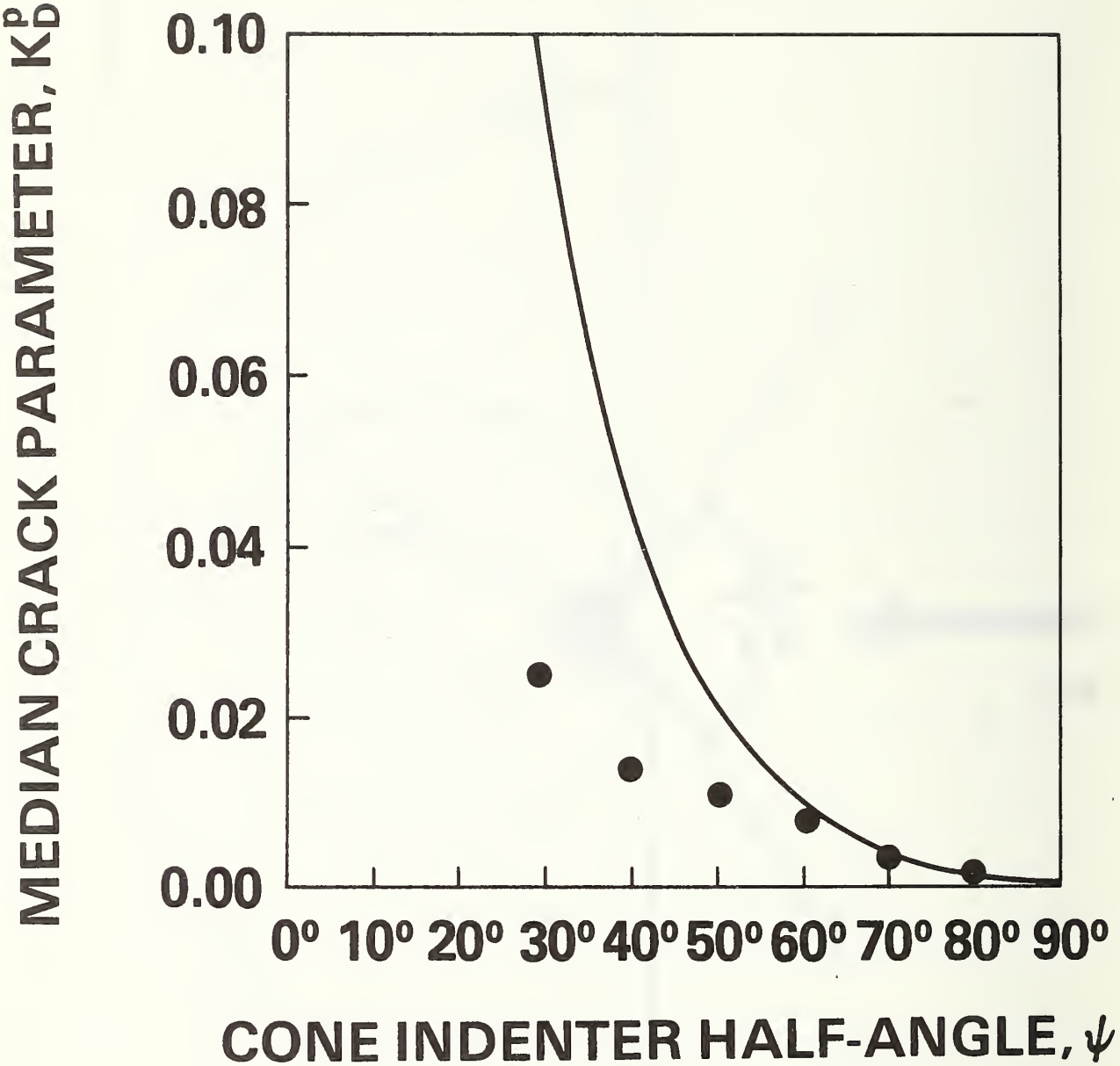
MEDIAN CRACK PARAMETER, K_D^p
0.10
0.08
0.06
0.04
0.02
0.00
0° 10° 20° 30° 40° 50° 60° 70° 80° 90°
CONE INDENTER HALF-ANGLE, ψ

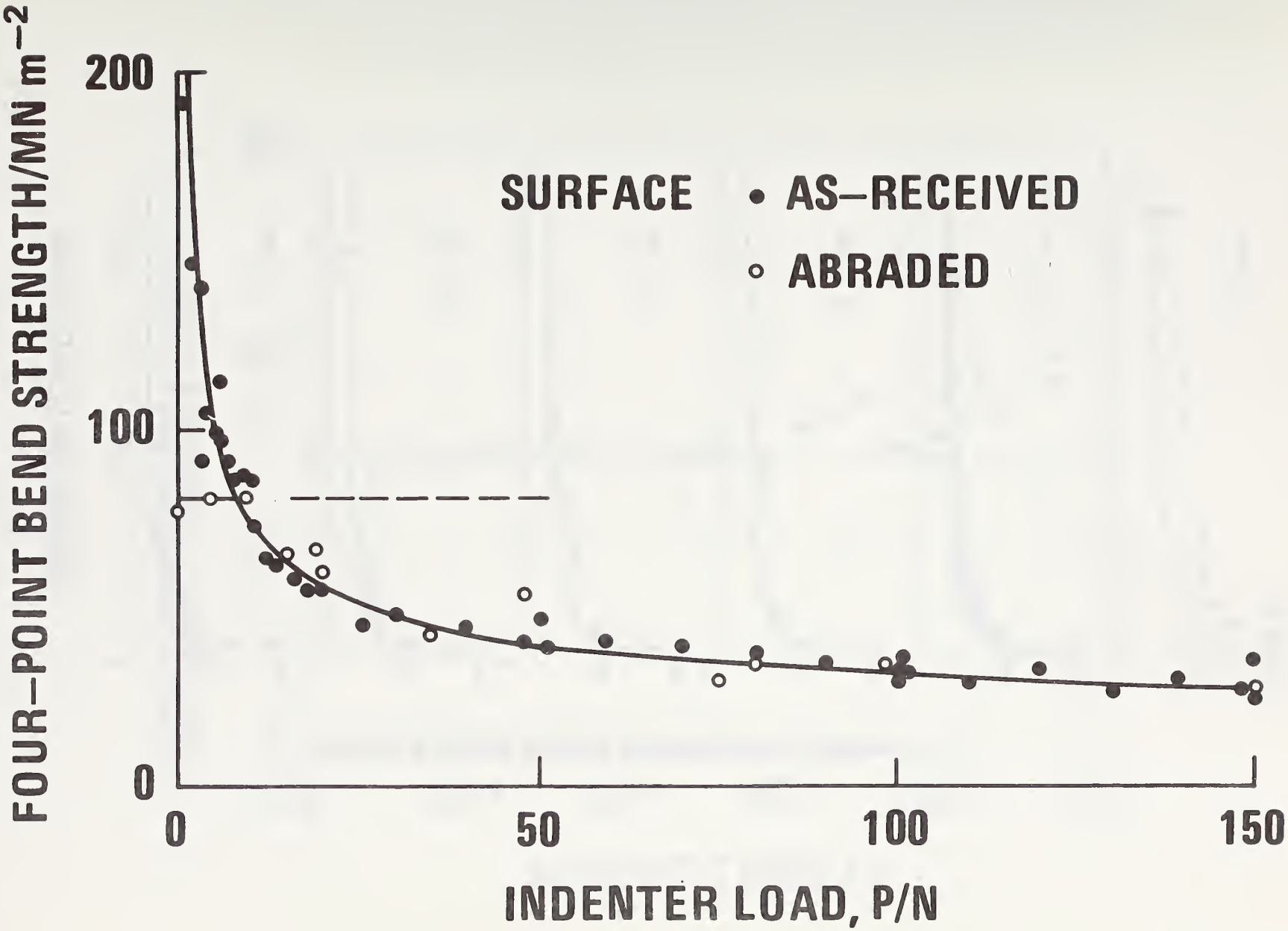
FOUR–POINT BEND STRENGTH/MN m^{-2}
200
100
0
SURFACE
• AS–RECEIVED
◦ ABRADED
0
50
100
150
INDENTER LOAD, P/N

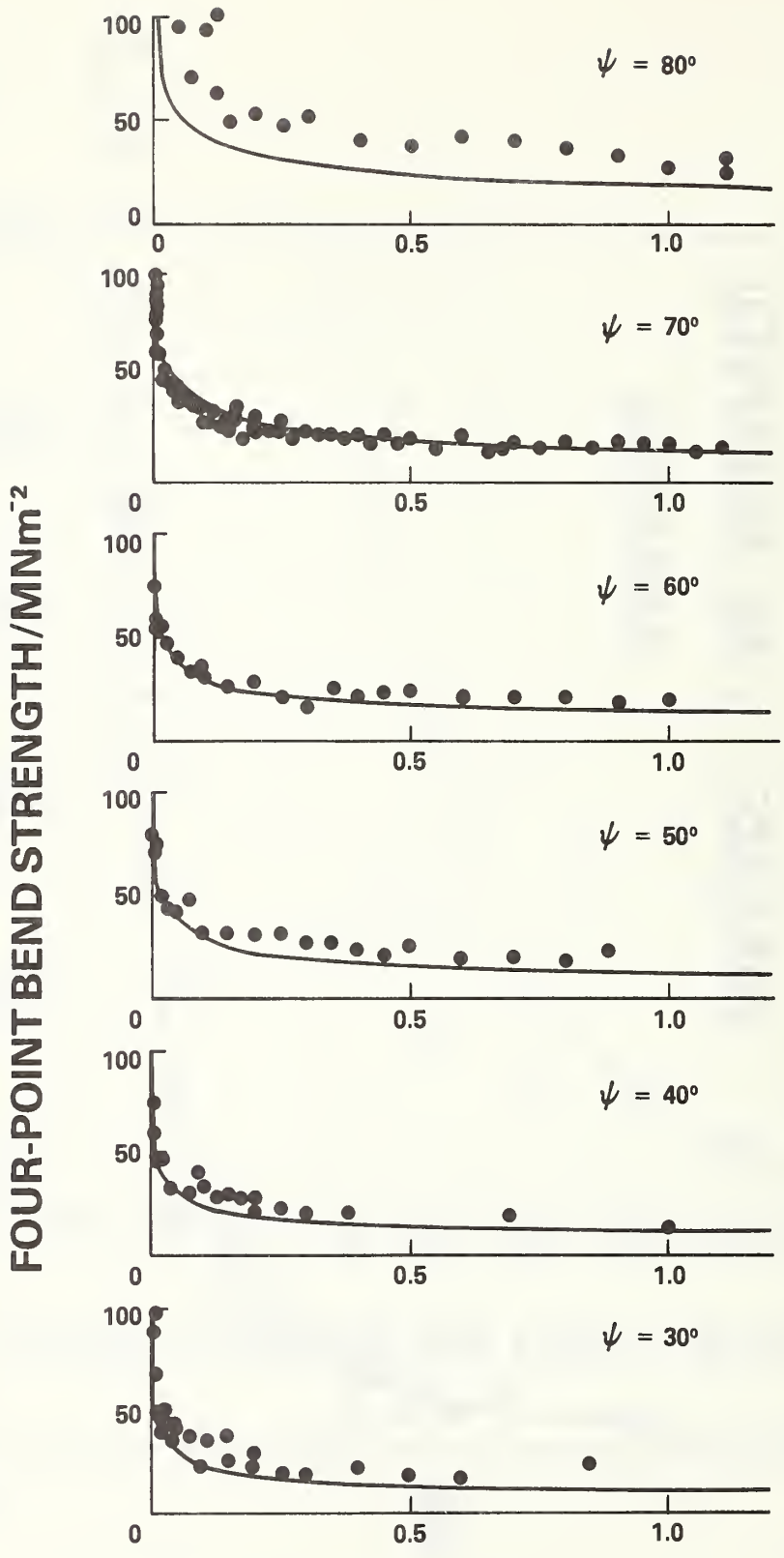
FOUR-POINT BEND STRENGTH/MNm^{-2}
100
50
0
0
0.5
1.0
ψ = 80°
ψ = 70°
ψ = 60°
ψ = 50°
ψ = 40°
ψ = 30°
INDENTER LOAD, P/kN

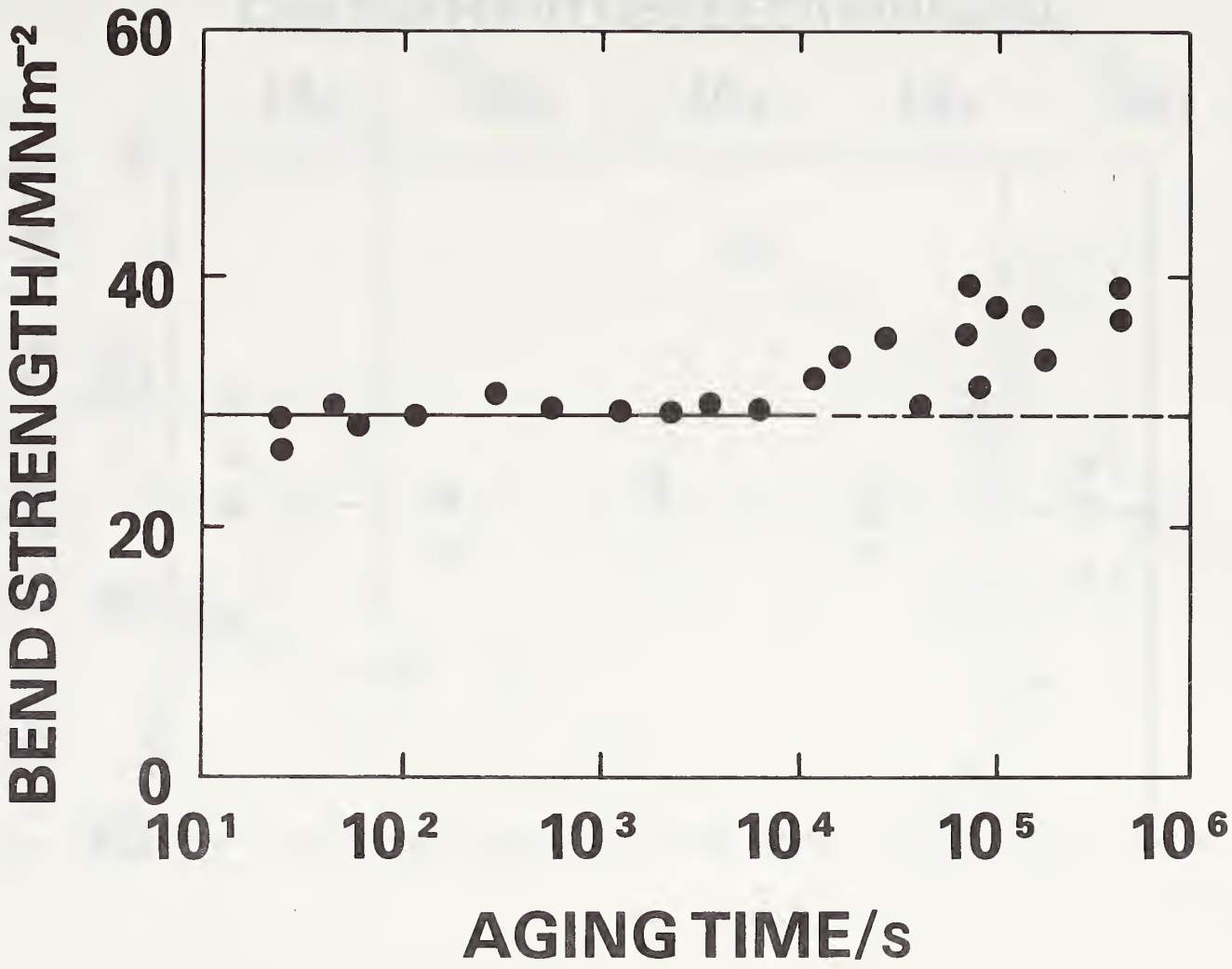
BEND STRENGTH/MNm⁻²
60
40
20
0
10¹
10²
10³
10⁴
10⁵
10⁶
AGING TIME/s

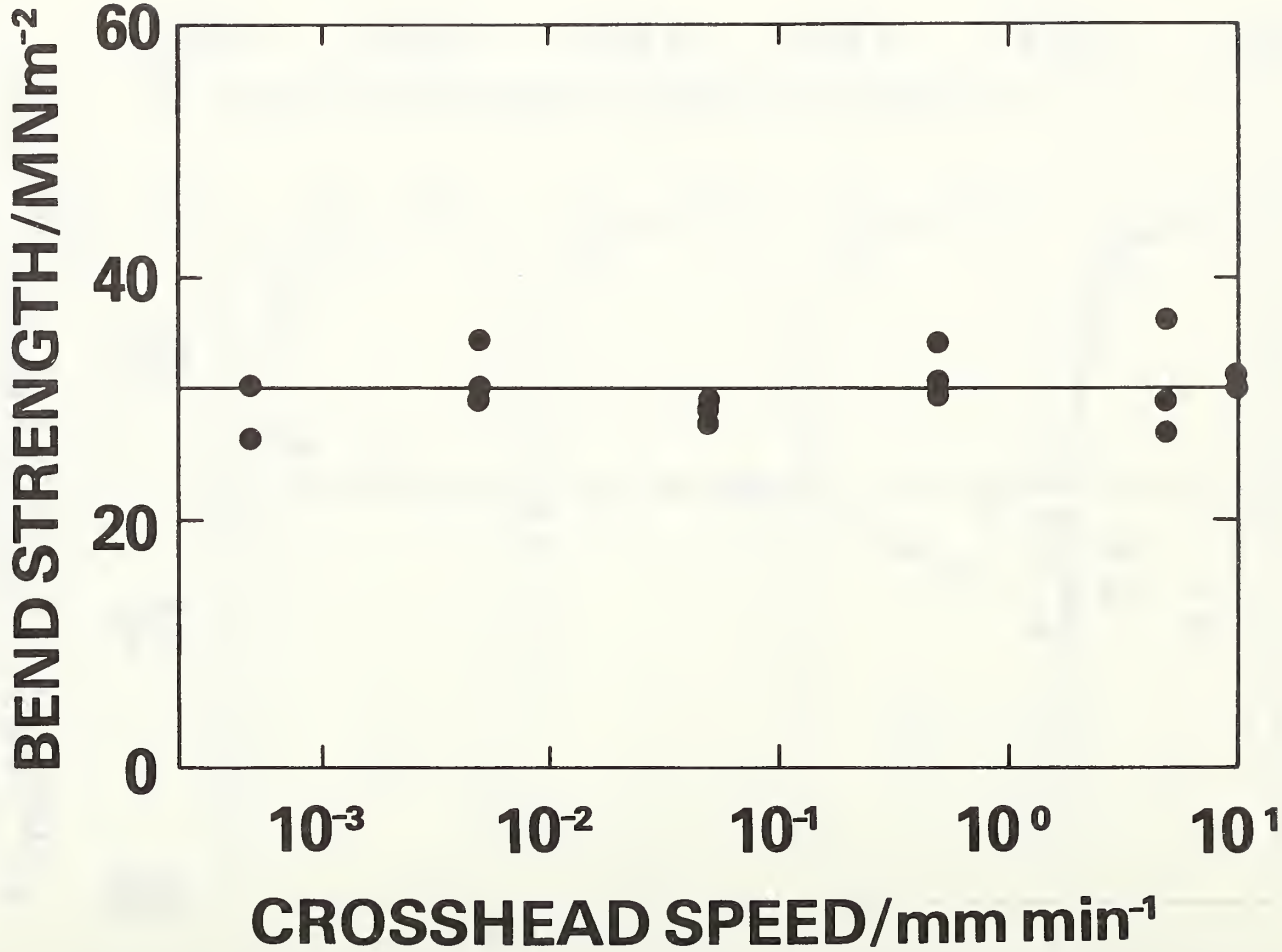
BEND STRENGTH/MNm^{-2}
60
40
20
0
10^{-3}
10^{-2}
10^{-1}
10^{0}
10^{1}
CROSSHEAD SPEED/mm min^{-1}

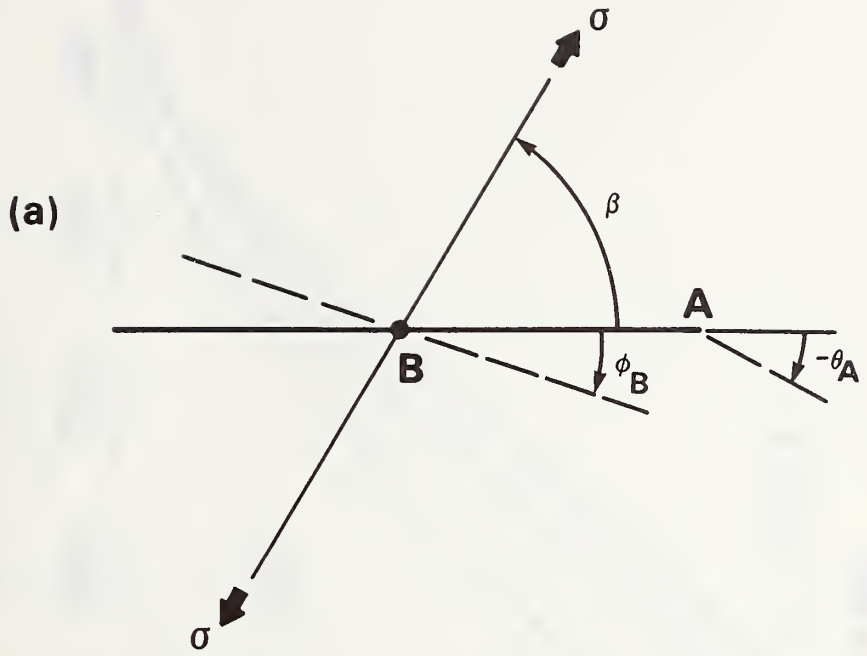
(a)
σ
β
A
B
ϕ_B
$-\theta_A$
σ

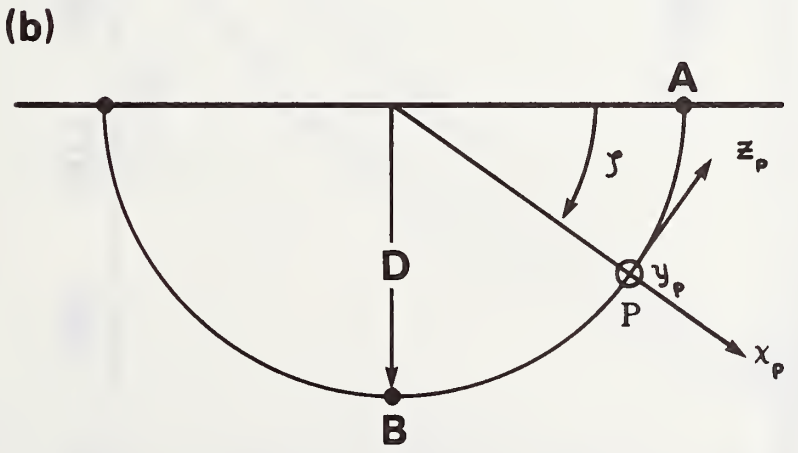
(b)
A
z_p
y_p
D
P
x_p
B

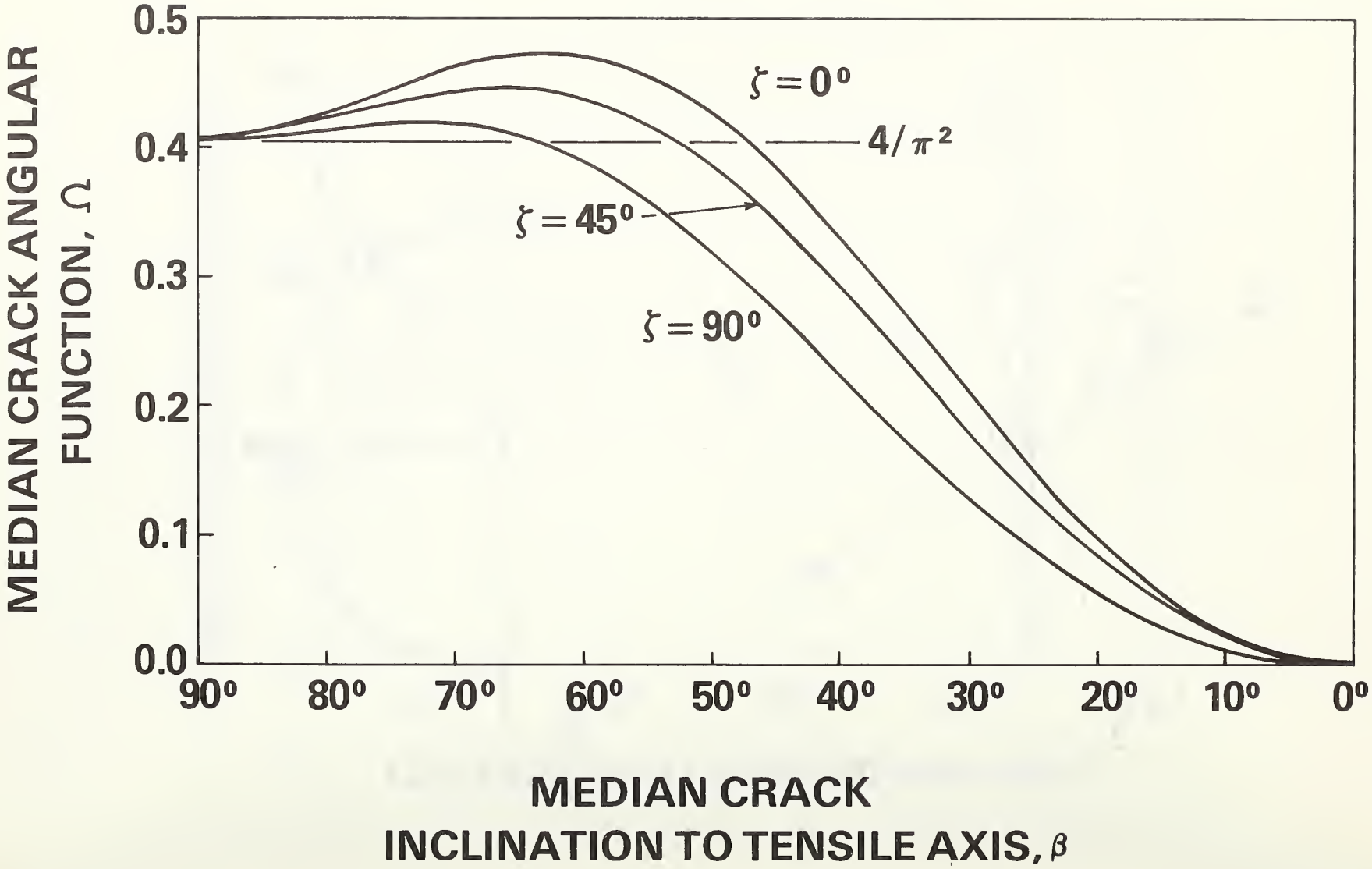
MEDIAN CRACK ANGULAR FUNCTION, Ω
0.5
0.4
0.3
0.2
0.1
0.0
ζ = 0°
4/π²
ζ = 45°
ζ = 90°
90°
80°
70°
60°
50°
40°
30°
20°
10°
0°
MEDIAN CRACK
INCLINATION TO TENSILE AXIS, β

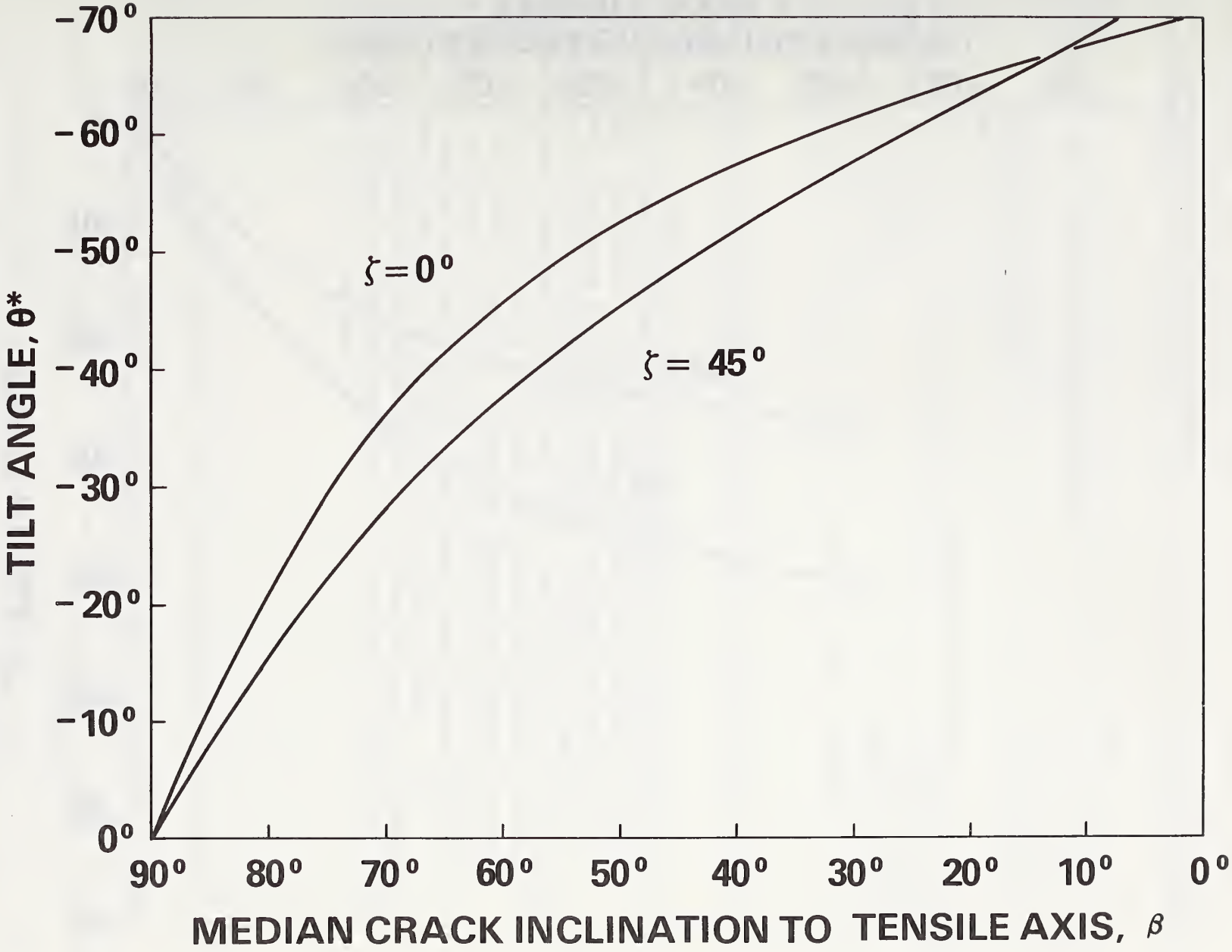
−70°
−60°
−50°
−40°
−30°
−20°
−10°
0°
TILT ANGLE, θ*
ζ = 0°
ζ = 45°
90°
80°
70°
60°
50°
40°
30°
20°
10°
0°
MEDIAN CRACK INCLINATION TO TENSILE AXIS, β

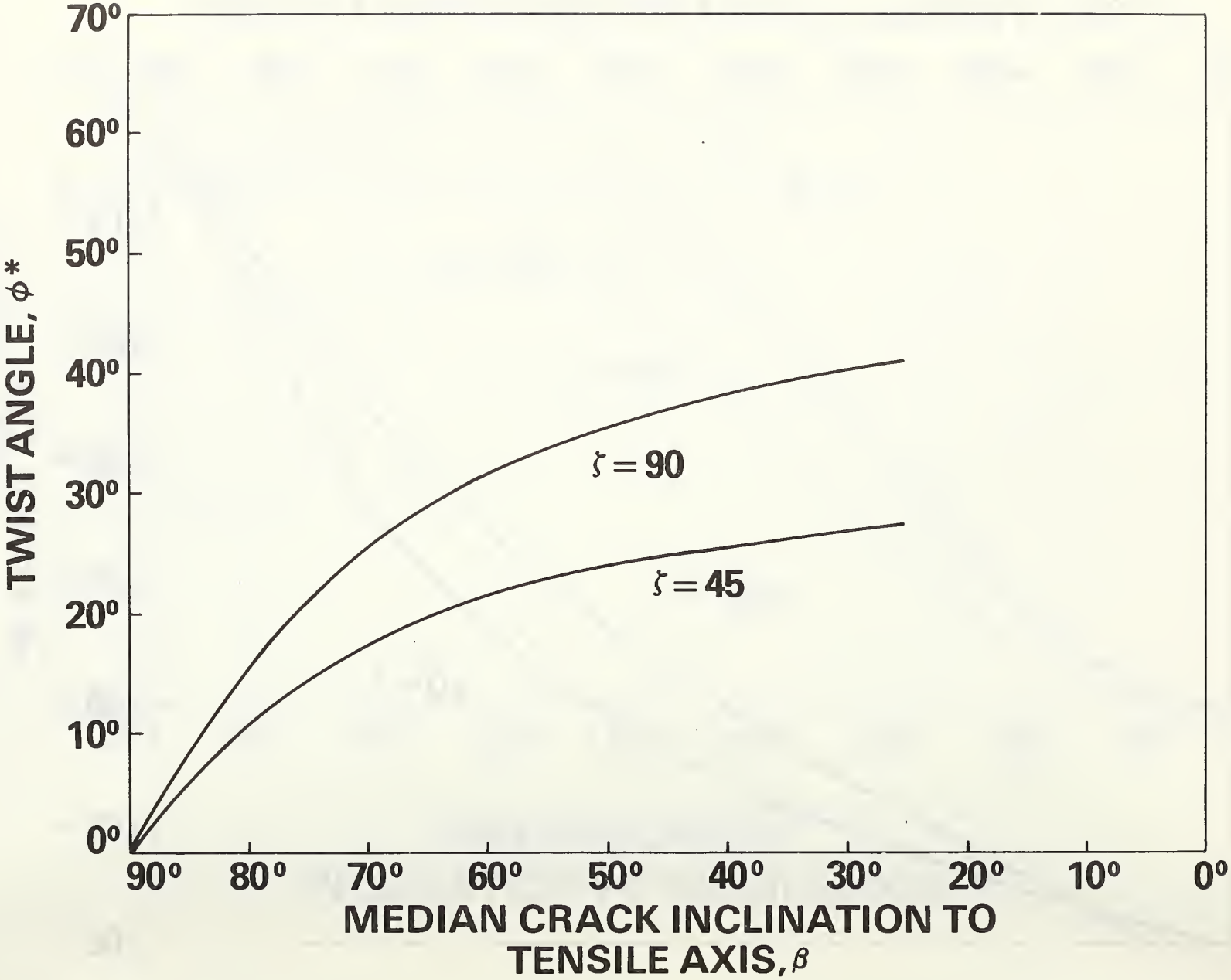
70°
60°
50°
40°
30°
20°
10°
0°
TWIST ANGLE, φ*
ζ = 90
ζ = 45
90° 80° 70° 60° 50° 40° 30° 20° 10° 0°
MEDIAN CRACK INCLINATION TO TENSILE AXIS, β

NBS-114A (REV. 7-73)

U.S. DEPT. OF COMM. BIBLIOGRAPHIC DATA SHEET	1. PUBLICATION OR REPORT NO. NBSIR 75-661	2. Gov't Accession No.	3. Recipient's Accession No.

4. TITLE AND SUBTITLE

Strength Degradation of Brittle Surfaces: Sharp Indenters

5. Publication Date: April 1975

6. Performing Organization Code

7. AUTHOR(S)

B. R. Lawn, E. R. Fuller, and S. M. Wiederhorn

8. Performing Organ. Report No.

9. PERFORMING ORGANIZATION NAME AND ADDRESS

NATIONAL BUREAU OF STANDARDS
DEPARTMENT OF COMMERCE
WASHINGTON, D.C. 20234

10. Project/Task/Work Unit No. 3130453

11. Contract/Grant No.

12. Sponsoring Organization Name and Complete Address *(Street, City, State, ZIP)*

Department of the Navy
Office of Naval Research
Arlington, Virginia 22217

13. Type of Report & Period Covered: Interim 7/74 - 6/30/75

14. Sponsoring Agency Code: ONR

15. SUPPLEMENTARY NOTES

16. ABSTRACT *(A 200-word or less factual summary of most significant information. If document includes a significant bibliography or literature survey, mention it here.)*

A theory of strength loss for brittle surfaces in contact situations, developed in a previous paper for "blunt" indenters, is here extended to the case of "sharp" indenters. A prior fracture mechanics analysis of crack growth beneath ideal cone indenters serves as the basis for predetermining the prospective surface degradation of ceramic components in service. Compared to blunt indenters, severe degradation can occur at the lower contact loads. However, at high loads the extent of degradation becomes remarkably insensitive to indenter geometry. Essential theoretical predictions are verified by bend tests on glass slabs. The effect of indenter "sharpness" and initial specimen surface flaw state are investigated systematically, along with some secondary rate effects in the contact process. The possibility of minimizing degradation via adjustment of material parameters (including hardness) or surface condition (e.g., residual stresses, frictional properties) is briefly discussed.

17. KEY WORDS *(six to twelve entries; alphabetical order; capitalize only the first letter of the first key word unless a proper name; separated by semicolons)*

Brittle solids; ceramic surfaces; degradation; fracture; indentation; strength

18. AVAILABILITY

[xx] Unlimited

[ ] For Official Distribution. Do Not Release to NTIS

[ ] Order From Sup. of Doc., U.S. Government Printing Office Washington, D.C. 20402, SD Cat. No. C13

[X] Order From National Technical Information Service (NTIS) Springfield, Virginia 22151

19. SECURITY CLASS (THIS REPORT)	21. NO. OF PAGES
UNCLASSIFIED	37
20. SECURITY CLASS (THIS PAGE)	22. Price
UNCLASSIFIED	$3.75

USCOMM-DC 29042-P74

INSTRUCTIONS

FORM NBS-114A: BIBLIOGRAPHIC DATA SHEET (REVERSE SIDE). This Bibliographic Data Sheet is an NBS adaptation of the form prescribed by COSATI guidelines (Appendix F. NBS Manual for Scientific and Technical Communications). Please complete with extreme care. This sheet will provide the basis for the literature citation of the publication, and in most cases it will become an integral part of the final publication itself.

A. Complete item 1 if information is available; otherwise, OTP will complete later. If non-NBS publication, state:"see item 15". (Additional instructions under K below.)

B. Ignore items 2, 3, 6, and 14; these are reserved for possible future use.

C. Complete items 4 and 7. When NBS-114A is resubmitted these items must be as they will actually appear on the published paper.

D. Leave items 5, 21, and 22 blank; OTP will complete.

E. Items 9, 19, and 20 are preprinted; you need add nothing.

F. Complete items 10, 11, and/or 12 when applicable. If no sponsor is involved, in item 12 state: same as item 9.

G. For item 13, enter "Final" or "Interim" and calendar period covered, as appropriate.

H. For item 15, enter other relevant information. (For example, upon receipt of completed Form NBS-266 from author, OTP will enter the complete citation for NBS-authorized papers published in non-NBS media.)

I. Complete items 16 and 17. Guidance is given in Section 4 and Appendix B of the NBS Manual for Scientific and Technical Communications. The abstract must agree with the one of the published paper.

J. For item 18, indicate one of the following: "Unlimited" - for open-literature documents cleared under NBS editorial procedures, or "For official distribution. Do not release to NTIS" - for limited, restricted, or need-to-know material. (See 5.1.4.2.1 of Brady memo dated January 16, 1973 "Reports to Sponsors.")

K. In completing item 1, use the brief designators shown in the right-hand column below. Each designator will be followed by the specific publication number for that item. This number will be the same in both the longer and briefer designators for the same document. For example: NBS Technical Note 548 will be equivalent to NBS TN-548. You would enter NBS TN-548 in item 1 of Form NBS-114A.

NBS Identification

NBS Technical Note	NBS TN-
NBS Monograph	NBS MN-
NBS Handbook	NBS HB-
NBS Special Publication	NBS SP-
NBS Applied Mathematics Series	NBS AMS-
NBS National Standard Reference Data Series	NBS NSRDS-
NBS Building Science Series	NBS BSS-
NBS Federal Information Processing Standards Publication	NBS FIPS-
NBS Voluntary Product Standards	NBS PS-
NBS Consumer Information Series	NBS CIS-
NBS Journal of Research Section A	NBS JRA-
NBS Journal of Research Section B	NBS JRB-
NBS Dimensions	NBS D-
NBS Interagency or Internal Report *	NBS IR-

Since each paper in the two volume NBS Journal of Research is assigned a specific designator, OTP will add appropriate Journal designator for item 1.

*If the outside sponsor assigned his own number, enter his number in item 1, and the NBSIR number in item 8.